

# Sources and Processes Affecting Fine Particulate Matter Pollution over North China: An Adjoint Analysis of the Beijing APEC Period

Lin Zhang,<sup>\*,†</sup> Jingyuan Shao,<sup>†</sup> Xiao Lu,<sup>†</sup> Yuanhong Zhao,<sup>†</sup> Yongyun Hu,<sup>†</sup> Daven K. Henze,<sup>‡</sup> Hong Liao,<sup>§</sup> Sunling Gong,<sup>||</sup> and Qiang Zhang<sup>⊥</sup>

<sup>†</sup>Laboratory for Climate and Ocean-Atmosphere Sciences, Department of Atmospheric and Oceanic Sciences, School of Physics, Peking University, Beijing 100871, China

<sup>‡</sup>Department of Mechanical Engineering, University of Colorado, Boulder, Colorado 80309, United States

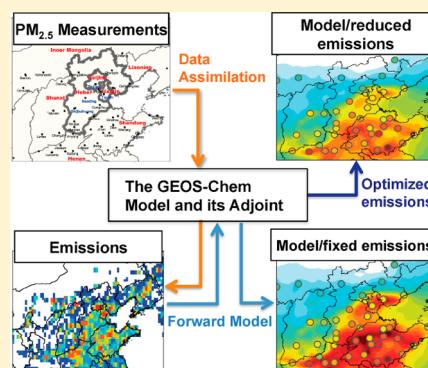
<sup>§</sup>School of Environmental Science and Engineering, Nanjing University of Information Science & Technology, Nanjing 210044, China

<sup>||</sup>Key Laboratory for Atmospheric Chemistry, Chinese Academy of Meteorological Sciences, CMA, Beijing, China

<sup>⊥</sup>Ministry of Education Key Laboratory for Earth System Modeling, Center for Earth System Science, Tsinghua University, Beijing 100084, China

## S Supporting Information

**ABSTRACT:** The stringent emission controls during the APEC 2014 (the Asia-Pacific Economic Cooperation Summit; November 5–11, 2014) offer a unique opportunity to quantify factors affecting fine particulate matter (PM<sub>2.5</sub>) pollution over North China. Here we apply a four-dimensional variational data assimilation system using the adjoint model of GEOS-Chem to address this issue. Hourly surface measurements of PM<sub>2.5</sub> and SO<sub>2</sub> for October 15–November 14, 2014 are assimilated into the model to optimize daily aerosol primary and precursor emissions over North China. Measured PM<sub>2.5</sub> concentrations in Beijing average 50.3 μg m<sup>-3</sup> during APEC, 43% lower than the mean concentration (88.2 μg m<sup>-3</sup>) for the whole period including APEC. Model results attribute about half of the reduction to meteorology due to active cold surge occurrences during APEC. Assimilation of surface measurements largely reduces the model biases and estimates 6%–30% lower aerosol emissions in the Beijing–Tianjin–Hebei region during APEC than in late October. We further demonstrate that high PM<sub>2.5</sub> events in Beijing during this period can be occasionally contributed by natural mineral dust, but more events show large sensitivities to inorganic aerosol sources, particularly emissions of ammonia (NH<sub>3</sub>) and nitrogen oxides (NO<sub>x</sub>) reflecting strong formation of aerosol nitrate in the fall season.



## 1. INTRODUCTION

Rapid industrialization and urbanization in China has led to rapid growth in emissions of air pollutants. The resulting severe air pollution has become one of the greatest environmental concerns in China.<sup>1–3</sup> In particular, the record-high haze events occurring in January 2013 over eastern and northern China have drawn worldwide attention on PM<sub>2.5</sub> (particulate matter with aerodynamic diameter less than or equal to 2.5 μm), the major air pollutant of haze.<sup>3–6</sup> Due to its fine size, PM<sub>2.5</sub> can be inhaled deeply into the lungs, causing adverse effects on human health including respiratory diseases and premature mortality.<sup>7–9</sup> It also impacts the atmospheric visibility and climate through scattering or absorbing the solar radiation and acting as cloud condensation nuclei.<sup>10,11</sup>

The North China Plain, particularly the Beijing–Tianjin–Hebei (BTH) region, is facing urgent need to control high PM<sub>2.5</sub> air pollution. Figure S1 (Supporting Information) shows the topography of the North China Plain and locations of the major cities in the region. It includes the mega-cities of Beijing

(the Capital of China) and Tianjin surrounded by Hebei, Shandong, and Shanxi provinces that are all heavily populated and industrialized. Beijing is located on the northwest of the North China Plain, with the west, north, and northeast directions adjacent to the Yanshan Mountain.<sup>1</sup> Annual averaged PM<sub>2.5</sub> concentration in Beijing reached 89.5 μg m<sup>-3</sup> in 2013, far exceeding the Chinese ambient air quality standard of 35 μg m<sup>-3</sup> for the annual PM<sub>2.5</sub> concentration.<sup>12</sup> In September 2013, the Chinese State Council issued the “Action Plan on Air Pollution Prevention and Control”, which set a strict target for the BTH region with the PM<sub>2.5</sub> concentrations to be reduced 25% by 2017 relative to 2012.<sup>13</sup> Achieving this target requires a better understanding of the factors affecting PM<sub>2.5</sub> air pollution over the BTH region.

Received: June 15, 2016

Accepted: July 19, 2016

Published: July 19, 2016

PM<sub>2.5</sub> includes directly emitted primary aerosols as well as secondary aerosols that are produced in the atmosphere through chemistry of precursor gases. A number of studies have examined the sources contributing to the PM<sub>2.5</sub> air pollution over the North China Plain using trajectory clustering,<sup>4,14</sup> measurement-based receptor models such as positive matrix factorization,<sup>3,4</sup> and sensitivity simulations with a chemical transport model.<sup>5,15</sup> However, considerable discrepancies exist in current estimates of the source contributions, including the relative importance of local production versus regional transport,<sup>14,16</sup> and contributions from different emission sectors.<sup>4,12</sup> These methods generally fail to fully consider the nonlinear chemistry of aerosol formation and transport processes, or ignore uncertainties in the model simulations such as those owing to uncertainties in the emissions used in the model. In this study, we will apply a four-dimensional variational (4D-Var) data assimilation system using the GEOS-Chem chemical transport model and its adjoint model to overcome these limitations.

Chemical transport models are valuable tools for investigating air pollution, and evaluation using in situ measurements is an important and routine component of their application. Somewhat less routine, and more challenging, is evaluation of the source-receptor relationships in such models. Such relationships are critical for informing air quality decision-making, but routine monitoring alone is insufficient to verify them. Fortunately, there are occasionally unique opportunities to test model estimates of how air pollution responds to emission changes. These include several cases offered by the temporary emission control measures enforced by the Chinese government to ensure good air quality for major events, e.g., the Sino-African Summit in early November 2006,<sup>17,18</sup> the Beijing 2008 Summer Olympic Games.<sup>19–22</sup> More recently, Beijing held the Asia-Pacific Economic Cooperation (APEC) Summit on November 5–11, 2014. Stringent emission control measures were applied in Beijing and its surrounding regions during November 3–12, 2014 to improve air quality, in particular to reduce the PM<sub>2.5</sub> air pollution. These measures included the suspension of production by factories, cutting the number of on-road vehicles by half in Beijing and neighboring provinces, assigning holidays for public-sector employees, among other measures.<sup>23,24</sup> The resulting air quality in Beijing showed notable improvements during the APEC week, which is called the “APEC blue”. Quantifying the effectiveness of emission controls on PM<sub>2.5</sub> air pollution in this period will be of great value for future policy making.

Here we use a nested-grid version of the GEOS-Chem global chemical transport model (CTM) and its adjoint model<sup>15,25</sup> with horizontal resolution of  $1/4^\circ \times 5/16^\circ$  ( $\sim 25$  km) to interpret the surface PM<sub>2.5</sub> measurements from the China National Environmental Monitoring Center (CNEMC) during October 15–November 14, 2014 (before and during APEC). The CNEMC started to release real-time hourly concentrations of SO<sub>2</sub>, NO<sub>2</sub>, CO, ozone (O<sub>3</sub>), PM<sub>2.5</sub>, and PM<sub>10</sub> in 74 major Chinese cities in January 2013, which further increased to 189 cities in 2014. We assimilate the surface hourly PM<sub>2.5</sub> and SO<sub>2</sub> measurements into the GEOS-Chem model to optimize the aerosol primary and precursor emissions at daily time scale. This provides a top-down constraint on the magnitude of emission changes. Model sensitivity simulations are used to differentiate the impacts of emission reductions and meteorology on the PM<sub>2.5</sub> concentrations. We further examine the sensitivity of PM<sub>2.5</sub> concentration in Beijing to the optimized

emissions for an improved understanding of the sources contributing to Beijing's PM<sub>2.5</sub> in fall.

## 2. METHODOLOGY

**2.1. GEOS-Chem Forward Model.** We update and apply a 4D-Var data assimilation system using the GEOS-Chem chemical transport model (CTM) and its adjoint model. The GEOS-Chem CTM (<http://geos-chem.org>) is driven by GEOS-FP assimilated meteorological data from the NASA Global Modeling and Assimilation Office (GMAO). The GEOS-FP data are available with a temporal resolution of 3 h (1 h for surface variables and mixing depths) and a horizontal resolution of  $1/4^\circ \times 5/16^\circ$ . We use a nested-grid version of GEOS-Chem<sup>26,27</sup> with the native  $1/4^\circ \times 5/16^\circ$  horizontal resolution over the East Asia ( $70^\circ\text{E}$ – $140^\circ\text{E}$ ,  $15^\circ\text{N}$ – $55^\circ\text{N}$ ) and  $2^\circ \times 2.5^\circ$  over the rest of the world.

The model includes a detailed tropospheric ozone-NO<sub>x</sub>-hydrocarbon-aerosol chemistry as described by Park et al.<sup>28</sup> and Mao et al.<sup>29</sup> Aerosol and gas-phase chemistry are coupled through heterogeneous aerosol chemistry parametrized as reactive uptake coefficients,<sup>30</sup> aerosol effects on photolysis rates,<sup>31</sup> and gas-aerosol partitioning of total NH<sub>3</sub> and HNO<sub>3</sub> calculated with the RPMARES thermodynamic equilibrium model.<sup>32</sup> Model simulated PM<sub>2.5</sub> includes aerosol sulfate, nitrate, ammonium, black carbon (BC), organic carbon (OC), and fine dust. BC and OC are emitted in hydrophobic forms, and converted to hydrophilic forms subject to wet deposition with an e-folding time of 1 day.<sup>33,34</sup> Mineral dust in the model is distributed in four-size bins (radii 0.1–1.0, 1.0–1.8, 1.8–3.0, and 3.0–6.0 μm) with the natural mineral dust emissions computed online using the mobilization scheme described by Fairlie et al.<sup>35</sup> Wet deposition of aerosols follows the scheme of Liu et al.,<sup>36</sup> and dry deposition is calculated with a standard resistance-in-series model as described by Wesely<sup>37</sup> for gases and Zhang et al.<sup>38</sup> for aerosols.

Global anthropogenic and natural emissions in the model follow our previous studies on the U.S. background ozone and nitrogen deposition.<sup>39,40</sup> For anthropogenic emissions over China, we use the Multiresolution Emission Inventory of China for the year 2010 (MEIC; <http://www.meicmodel.org>) developed by Tsinghua University<sup>41,42</sup> except for NH<sub>3</sub> emissions that are from the REAS-v2 inventory<sup>43</sup> but with an improved seasonal variability as described in Zhao et al.<sup>44</sup> Following Zhu et al.<sup>45</sup> the NH<sub>3</sub> emissions from fertilizer use and livestock are increased by 90% in the daytime and reduced by 90% at night to account for the diurnal variability. The anthropogenic primary PM<sub>2.5</sub> emissions described by Lei et al.<sup>42</sup> are implemented as the fine dust in the model.<sup>15</sup> This anthropogenic primary PM<sub>2.5</sub> is mainly fine dust emitted together with BC and OC from combustion activities, and it does not include fugitive dust. Figure S2 shows the spatial distribution of anthropogenic emissions of NO<sub>x</sub>, SO<sub>2</sub>, NH<sub>3</sub>, black carbon (BC), organic carbon (OC), and fine dust in October over the North China Plain. With the fine horizontal resolution of  $1/4^\circ \times 5/16^\circ$  ( $\sim 25$  km), the model better resolves the heterogeneous emission patterns. High emission rates of those pollutants generally correspond to the locations of the cities, except for NH<sub>3</sub> emissions which are mainly from agricultural activities.

Formation of secondary organic aerosols (SOA) as simulated by the GEOS-Chem model is found to be severely underestimated in China likely due to missing precursor emissions or formation pathways.<sup>46</sup> Further developments to the SOA

simulation in GEOS-Chem to include SOA from semivolatile and intermediate volatile organic compounds<sup>47</sup> lead to lower global SOA burdens, and have not been extensively evaluated in China. Thus, we do not simulate SOA in the model for this study; instead, we include an estimate of SOA mass in the model's total PM<sub>2.5</sub> using measured SOA/POA (primary organic aerosols) ratios. Submicron aerosol (PM<sub>1</sub>) measurements conducted by Sun et al.<sup>48</sup> in the north of Beijing during October 15–November 13, 2014 showed that SOA account for 17%–23% of the surface PM<sub>1</sub> concentrations with SOA/POA ratios ranging 1.28–2.0 before APEC and 0.52–0.61 during APEC. Concurrent aerosol measurements reported by Zhang et al.<sup>24</sup> found similar SOA mass contributions with SOA/POA ratios of 1.56 before APEC and 1.0 during APEC. Here we estimate SOA by scaling simulated OC with the measured mean SOA/POA ratios from the two studies (1.57 before APEC for all model simulations and 0.71 during APEC in the optimized simulation). While we acknowledge that large uncertainties exist in the estimated SOA concentration by ignoring the SOA sources and chemical processes which are highly dependent on atmospheric conditions, this approach provides a relatively unbiased estimate of total PM<sub>2.5</sub> for our adjoint analysis and thus mitigates the impact of neglecting SOA on the source attribution for the other aerosol components presented here. As our understanding of SOA matures, future studies may better quantify the impact of SO<sub>2</sub> and NO<sub>x</sub> emissions on catalyzing SOA formation;<sup>49,50</sup> at present, estimates of the contributions of these species to PM<sub>2.5</sub> may instead be considered a lower bound.

Previous studies have also shown that the GEOS-Chem model tends to overestimate surface concentrations of aerosol nitrate most likely due to high biases in simulated HNO<sub>3</sub> concentrations.<sup>39,51,52</sup> Here we follow Heald et al.<sup>51</sup> by lowering the simulated HNO<sub>3</sub> concentrations by 25% in the model to correct the nitrate bias. While overestimates of NO<sub>x</sub> emissions in the model could also cause the high nitrate bias, comparisons of simulated versus measured tropospheric NO<sub>2</sub> columns during this period (as will be discussed in Figure S3) indicate the NO<sub>x</sub> emissions are reasonable.

## 2.2. Data Assimilation Based on the Adjoint Model.

The adjoint of GEOS-Chem, first developed by Henze et al.,<sup>25</sup> includes components of transport, gas-phase chemistry, and heterogeneous chemistry to fully represent the aerosol simulation.<sup>25,53</sup> It has been tested and applied in a number of studies to quantify aerosol sensitivities and to improve aerosol emission estimates.<sup>25,45,53–55</sup> Our previous work has extended the GEOS-Chem adjoint to the fine 1/4° × 5/16° horizontal resolution and applied it to quantify the sources of wintertime PM<sub>2.5</sub> over the North China Plain.<sup>15</sup>

We use the GEOS-Chem adjoint model to provide a framework of data assimilation combining measurements and the model to optimize the aerosol emissions. The forward model can mathematically viewed as a numerical operator  $F$ :  $y_{n+1} = F(y_n, x)$ , where  $y_n$  is the vector of all tracer concentrations at time step  $n$ , and  $x$  is the vector of model variables to be optimized, such as emissions. This optimization is accomplished by minimizing the cost function ( $J$ ), given by the following:

$$J(x) = (F(x) - y_{\text{obs}})^T S_e^{-1} (F(x) - y_{\text{obs}}) + (x - x_a)^T S_a^{-1} (x - x_a) \quad (1)$$

Here  $y_{\text{obs}}$  is the vector of measurements,  $x_a$  is the vector of a priori emissions, and  $S_a$  and  $S_e$  are the error covariance matrices of the a priori and the observation system, respectively.

We use the CNEMC surface measurements of PM<sub>2.5</sub> and SO<sub>2</sub> (<http://113.108.142.147:20035/emcpublish/>) at 46 cities in North China, which includes 13 cities in the BTH region (Figure S1). Each city has several monitoring sites; here we have averaged them to each city for representing a regional condition and for comparison with the model. We do not use the NO<sub>2</sub> measurements at those sites in this study because they are monitored by the chemiluminescence analyzer equipped with a molybdenum converter that can overestimate NO<sub>2</sub> concentrations by more than 50% due to interferences from other nitrogen species.<sup>56</sup>

For each day of October 15–November 14, 2014, we conduct a separate inversion by assimilating the hourly CNEMC surface measurements of PM<sub>2.5</sub> and SO<sub>2</sub> for that day into the model to optimize the mean anthropogenic aerosol emissions averaged over a 5-day period backward (the vector  $x$  in eq 1) to account for the lifetime of surface PM<sub>2.5</sub>. The anthropogenic aerosol emissions include both primary (BC, OC, fine dust) and precursor species (SO<sub>2</sub>, NO<sub>x</sub>, NH<sub>3</sub>) as described above (Figure S2). We do not optimize natural mineral dust emissions because the source regions mainly locate in the western China, beyond our focused domain (Figure S1). A forward sensitivity simulation with natural mineral dust emissions turned off shows that there is one strong dust event impacting North China during this period (on October 17–18 as will be discussed below) and contributions of natural dust to PM<sub>2.5</sub> in Beijing are less than 1 μg m<sup>-3</sup> during APEC.

For the emission optimization, we assume the a priori error covariance ( $S_a$ ) to be uncorrelated, and the uncertainties to be 100% for NH<sub>3</sub> emissions and 50% for the other species, reflecting the uncertainties in their bottom-up estimates as well as the relative emission changes due to the control measures.<sup>21,41</sup> The observational error covariance ( $S_{\text{obs}}$ ) represents the sum of the measurement error, the representation error, and the forward model error.<sup>57</sup> We follow the relative residual error (RRE) method<sup>57</sup> and estimate the variance of the observational error based on the statistics of differences between measurements and model results with the a priori emissions. The observational errors are estimated to be 22–85 μg m<sup>-3</sup> for PM<sub>2.5</sub> and 16–96 μg m<sup>-3</sup> for SO<sub>2</sub> among the measurement sites.

The adjoint model of GEOS-Chem calculates the gradient of the cost function ( $\nabla_x J$ ) numerically. This gradient calculation is then used iteratively to minimize the cost function  $J$  with the quasi-Newton L-BFGS-B optimization routine.<sup>58</sup> The optimization is considered to have converged when the cost function decreases by less than 1% in consecutive iterations. It typically takes 10–12 iterations to converge, with values of the converged cost function reduced by 25–40%.

**2.3. Calculation of Adjoint Sensitivity of PM<sub>2.5</sub> to emissions.** The adjoint model is also used to calculate the sensitivities of PM<sub>2.5</sub> concentrations in Beijing to aerosol emissions at the model 1/4° × 5/16° resolution, using the emissions constrained from the 4D-Var data assimilations. The adjoint method provides a computationally efficient way to calculate the sensitivity of model variables (e.g., daily mean PM<sub>2.5</sub> concentration at a model grid cell denoted as  $H$ ) to all model parameters (e.g., emissions denoted as  $x$ ). Briefly, we

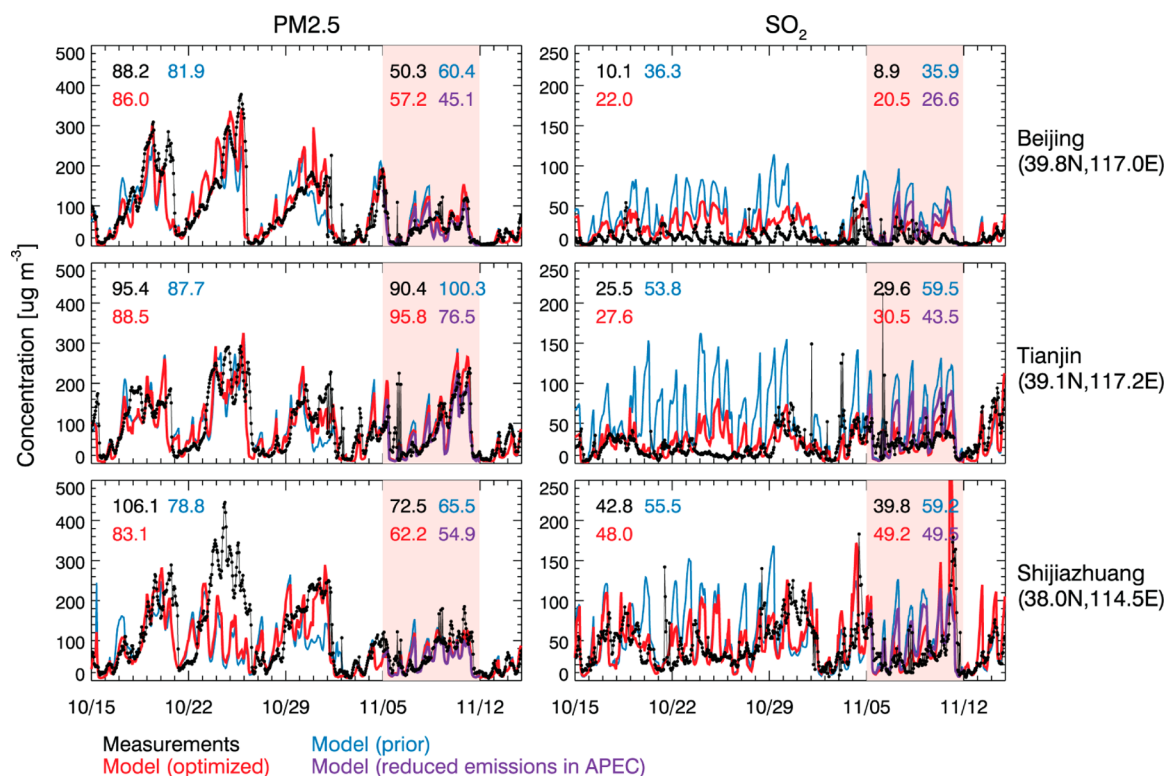


**Figure 1.** Time series of measured vs GEOS-Chem simulated hourly surface PM<sub>2.5</sub> (left panels) and SO<sub>2</sub> (right panels) concentrations at three cities: Beijing, Tianjin, and Shijiazhuang (see Figure 2 for their locations) during October 15–November 14, 2014. The shaded area represents the APEC time period (November 5–11). Measurements (dots and black lines) are compared with model results with prior emissions (blue lines) and with optimized emissions (red lines). Also shown is a sensitivity simulation with anthropogenic emissions over the Beijing–Tianjin–Hebei (BTH) region reduced by 30% in the APEC period (purple lines). Numbers inset are mean concentrations averaged over the time period and during APEC.

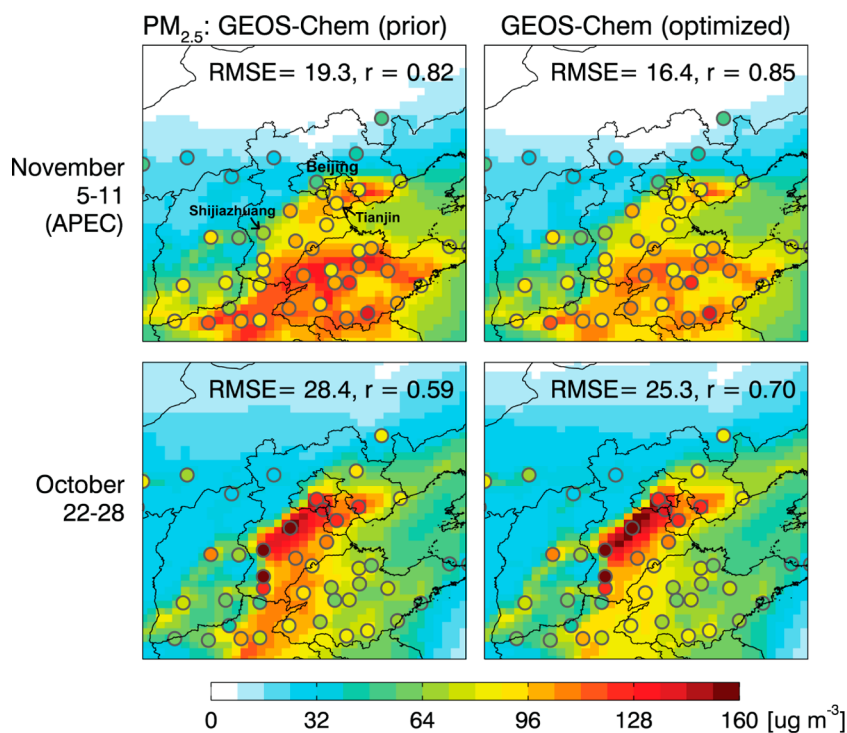


**Figure 2.** Surface mass concentrations of PM<sub>2.5</sub> averaged over 2 weeks: November 5–11 (the APEC week) and October 22–28, 2014. Measurements from CNEMC (circles) are overplotted over model simulations with the prior (left column) and optimized emissions (right column). The observation versus model correlation coefficient (*r*) and root-mean-square error (RMSE) are shown inset.

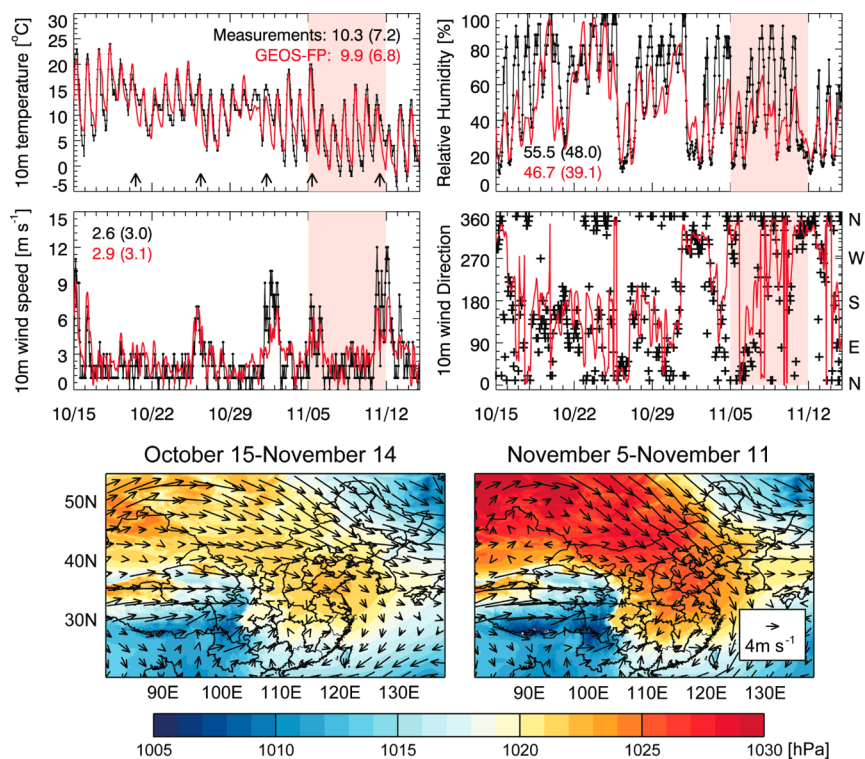


**Figure 3.** Comparison of measured (black) and GEOS-FP (red) hourly 10-m temperature, relative humidity (RH), 10-m wind speed and direction (top four panels) over the surface of Beijing during October 15–November 14, 2014. The shaded area denotes the APEC time period. Arrows in the first panel indicate the cold surges identified by rapid decreases in temperature and RH. Mean values for the whole period and for APEC (in parentheses) are shown inset. The bottom two panels show the GEOS-FP sea-level pressure with winds at 850 hPa overplotted averaged over this period (left) and the APEC week (right).

define the adjoint sensitivity variables as  $\lambda_{\mathbf{x}}^0 = \left(\frac{\partial H}{\partial \mathbf{x}}\right)^T$  representing the sensitivity of  $H$  to model emissions, and  $\lambda_{\mathbf{y}}^0 = \left(\frac{\partial H}{\partial \mathbf{y}_0}\right)^T$  representing its sensitivity to the initial conditions. The adjoint model computes the variables simultaneously backward in time following:

$$\lambda_{\mathbf{y}}^{n-1} = \left(\frac{\partial \mathbf{F}}{\partial \mathbf{y}}(\mathbf{y}_{n-1}, \mathbf{x})\right)^T \lambda_{\mathbf{y}}^n \quad (2)$$

$$\lambda_{\mathbf{x}}^{n-1} = \left(\frac{\partial \mathbf{F}}{\partial \mathbf{x}}(\mathbf{y}_{n-1}, \mathbf{x})\right)^T \lambda_{\mathbf{y}}^n + \lambda_{\mathbf{x}}^n \quad (3)$$

Here  $\left(\frac{\partial \mathbf{F}}{\partial \mathbf{y}}(\mathbf{y}_{n-1}, \mathbf{x})\right)^T$  and  $\left(\frac{\partial \mathbf{F}}{\partial \mathbf{x}}(\mathbf{y}_{n-1}, \mathbf{x})\right)^T$  are the transpose of the model Jacobian matrices with respect to  $\mathbf{y}_n$  and  $\mathbf{x}$ .

### 3. RESULTS AND DISCUSSION

**3.1. Measurements and Model Simulations in the APEC Period.** Figures 1 and 2 show the measured and model simulated  $\text{PM}_{2.5}$  and  $\text{SO}_2$  concentrations over the North China Plain. Figure 1 shows time series of hourly  $\text{PM}_{2.5}$  and  $\text{SO}_2$  concentrations at three cities (Beijing, Tianjin, and Shijiazhuang) in the BTH region during the period of October 15–November 14, 2014, and Figure 2 compares the spatial distribution of  $\text{PM}_{2.5}$  concentrations averaged for two one-week time periods: November 5–11, 2014 (APEC) and October 22–28, 2014. The spatial distribution of  $\text{SO}_2$  concentrations is shown in Figure S3. Measured  $\text{PM}_{2.5}$  concentrations in Beijing

averaged  $88.2 \mu\text{g m}^{-3}$  for this whole time period and were 43% lower ( $50.3 \mu\text{g m}^{-3}$ ) during the APEC week. Similar reductions of  $\text{PM}_{2.5}$  were shown at Tianjin and Shijiazhuang cities during APEC. As shown in Figure 2, comparing with averaged  $\text{PM}_{2.5}$  concentrations in late October, the reductions during APEC primarily occurred over the BTH region. Li et al.<sup>23</sup> also found that VOC concentrations over Beijing were reduced by 44% during APEC relative to the time periods before and after APEC.

The model simulations with the prior emissions and with the optimized emissions after assimilating the measurements are also shown in Figures 1 and 2. The prior model results simulate  $81.9 \mu\text{g m}^{-3}$  for the whole period and  $60.4 \mu\text{g m}^{-3}$  for APEC in Beijing. This simulated lower value during APEC explains about 56% ( $21.5 \mu\text{g m}^{-3}$ ) of the observed reduction, reflecting differences due to meteorology as will be discussed in the next section. The prior model results generally overestimate the measured  $\text{PM}_{2.5}$  concentrations during APEC, but underestimate their values averaged over the whole period. Assimilating the measurements into the model largely reduces the model biases. As we can see for Beijing, the model biases for  $\text{PM}_{2.5}$  are reduced by 65% (from  $-6.3$  to  $-2.2 \mu\text{g m}^{-3}$ ) in the whole period and by 32% (from  $+10.1$  to  $+6.9 \mu\text{g m}^{-3}$ ) in APEC. The optimized model results also show improved agreement with the measurements over the North China domain with higher correlation coefficients and lower root-mean-square errors (Figures 2 and S3).

The prior model overestimates  $\text{SO}_2$  measurements over Beijing and Tianjin by a factor of 2–3, while comparisons at other cities over the North China Plain show smaller model positive biases (Figure 1 and Figure S3). There might be several

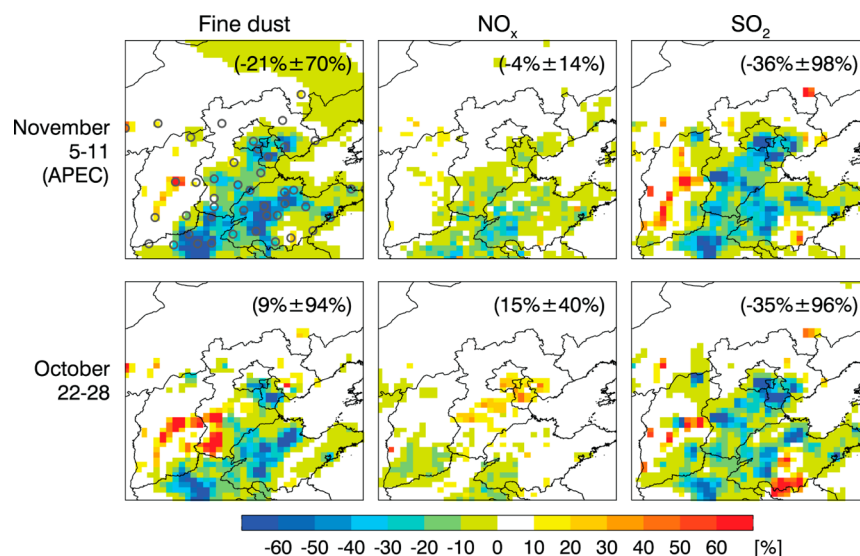


**Figure 4.** Correction factors in the optimized anthropogenic emissions of fine dust, NO<sub>x</sub>, and SO<sub>2</sub> relative to the prior emissions (Figure S2) averaged for November 5–11 (the APEC week) and October 22–28, 2014. Values in parentheses represent the total emission changes integrated over the BTH region. The gray circles in the top-left panel denote the locations of monitoring cities.

reasons causing the large model high biases at the two megacities. First, the model uses the MEIC anthropogenic emissions for the year 2010. SO<sub>2</sub> emissions in China have shown a decreasing trend in recent years mainly due to installation of flue gas desulfurization (FGD) systems at coal-fired power plants.<sup>59,60</sup> The trend is the largest over the North China Plain with SO<sub>2</sub> emissions in this region decreased by more than 20% within 2005–2010.<sup>60</sup> Second, the monitoring sites in the two megacities may not well represent a larger spatial area covered by the model horizontal resolution. Wang et al.<sup>61</sup> conducted ground-based MAX-DOAS measurements of SO<sub>2</sub> at a rural station near Beijing in 2010–2013. They reported monthly mean surface SO<sub>2</sub> concentrations in the range of 40–82 μg m<sup>-3</sup> (15–30 ppbv) in October and November, comparable to our model results of 35.9 μg m<sup>-3</sup> in Beijing. The model may also miss some chemical mechanisms or oxidants that oxidize SO<sub>2</sub> to sulfate<sup>62</sup> that requires further observational and modeling studies to identify.

Bottom-up estimates suggest that during the APEC period anthropogenic emissions are reduced by more than 40% in Beijing and by 30% in surrounding regions.<sup>63</sup> This is evident by satellite observations of tropospheric NO<sub>2</sub> columns that commonly used to constrain surface NO<sub>x</sub> emissions. Huang et al.<sup>64</sup> analyzed the OMI NO<sub>2</sub> column measurements and found that NO<sub>2</sub> column concentrations over Beijing and southern Hebei were 36% lower during APEC than those before APEC. Figure S4 shows OMI measured NO<sub>2</sub> tropospheric columns averaged over two time windows before (October 16–31, 2014) and during APEC (November 5–11, 2014), comparing to both prior and optimized GEOS-Chem model results applied with OMI averaging kernels. The OMI versus model discrepancies are distinctly different for the two periods. The simulated NO<sub>2</sub> tropospheric columns over the BTH region show on average a negative bias of -12% for October 16–31 but a positive bias of 9% for the APEC week, indicating NO<sub>x</sub> emission reductions during APEC. Model results with the optimized emissions show reduced model biases providing an independent evaluation of the inversion.

**3.2. Meteorological Variations and Emission Reductions.** Assessing the impact of emission reductions on the

PM<sub>2.5</sub> concentrations can be complicated by the variability of meteorological conditions. A prominent feature in Figure 1 is that PM<sub>2.5</sub> concentrations over the BTH cities show periods of about 7 days with PM<sub>2.5</sub> slowly accumulating in the first several days followed by a rapid decrease. This is determined by the episodic incursion of cold midlatitude air (“cold surges”) associated with the East Asian winter monsoon.<sup>65,66</sup> The cold surges are linked to the southeastward expansion of the Siberian high, and are most frequent in spring and fall.<sup>65</sup> Figure S5 illustrates the passage of a cold surge and its influences on the surface PM<sub>2.5</sub> concentrations over the North China Plain during November 4–7, 2014. On November 4, the daily mean PM<sub>2.5</sub> concentration in Beijing reached 124 μg m<sup>-3</sup> when the dominant surface winds over the BTH region were southwest. The winds switched to northwesterly over the next 2 days with the arrival of a cold surge and rapidly ventilated the pollution over this region. The daily mean PM<sub>2.5</sub> concentration in Beijing decreased to 13 μg m<sup>-3</sup> on November 6.

We show in Figure 3 measured and GEOS-FP data for temperature, relative humidity, wind speed and direction in Beijing during October 15–November 14, 2014. The meteorological measurements were obtained from the National Climatic Data Center (NCDC) of the National Oceanic and Atmospheric Administration (NOAA) (<http://gis.ncdc.noaa.gov/map/viewer/>). The GEOS-FP meteorological data for all four variables are in good agreement with the measurements with only small biases and correlation coefficients greater than 0.9. We follow Liu et al.<sup>66</sup> and simply define the occurrence of a cold surge as a rapid increase in surface pressure associated with decreases in surface temperature and relative humidity. As shown in Figure 3, about 5 cold surges can be identified in the time period. In particular, two cold surges occurred during the APEC period on November 5 and November 11, respectively. It leads to notable differences in the meteorological variables between the APEC period and the other weeks (*p*-values < 0.01), such as observed higher wind speed in APEC (3.0 m s<sup>-1</sup> vs 2.6 m s<sup>-1</sup> averaged for the whole period). This is also seen from the bottom two panels of Figure 3 by comparing the sea-level pressure and wind at 850 hPa averaged over the whole period and the APEC week, with higher sea-level pressure

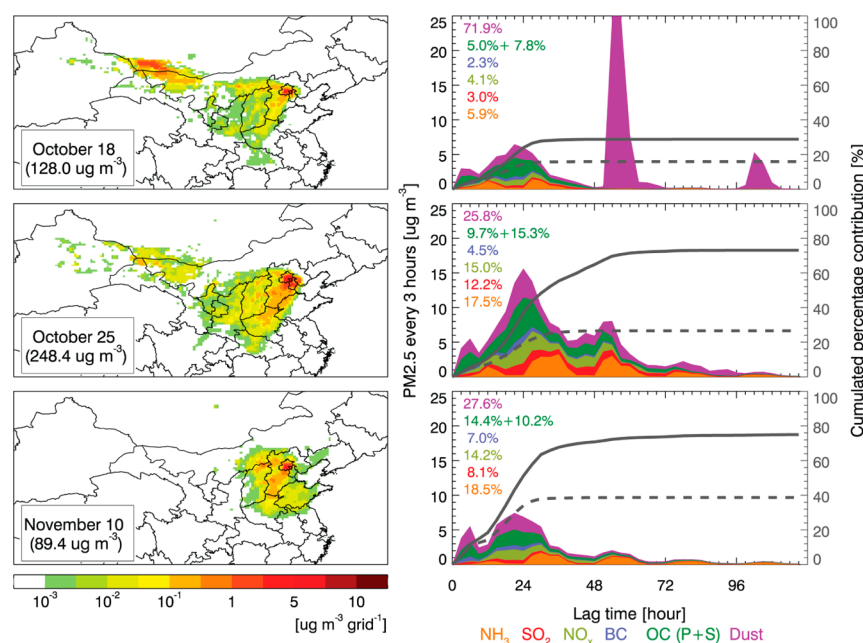


**Figure 5.** Sensitivity of surface daily  $\text{PM}_{2.5}$  concentrations in Beijing to the optimized aerosol primary and precursor ( $\text{NH}_3$ ,  $\text{SO}_2$ ,  $\text{NO}_x$ , BC, OC, and dust) emissions as computed by the GEOS-Chem adjoint model for three pollution events: October 18 (top panels), October 25 (central panels), and November 10, 2014 (bottom panels). Sensitivity to OC emissions are separated to primary (P) and secondary (S) OC based on measured POA/SOA ratios as described in the text. The left panels show the sensitivities integrated over time and chemical species at the model  $1/4^\circ \times 5/16^\circ$  grid resolution. The right panels show the time-dependent sensitivities (going backward in time and integrating over every 3 h) to emissions of different chemical species integrated over the model domain. The dashed and solid lines show cumulated percentage contributions from emissions in the Beijing municipality and in the BTH region, respectively.

associated with stronger northwest wind in APEC due to the more active cold surges. We have shown above (Figure 1) that model results with prior emissions (fixed in time) simulate about 56% ( $21.5 \mu\text{g m}^{-3}$ ) of the observed  $\text{PM}_{2.5}$  reduction in Beijing during APEC, which differentiates the impact of meteorology on air pollution.

Assimilation of the surface measurements into the model provides a top-down estimation of the emissions-driven changes in air pollutants with the different meteorological conditions fully considered. Figure 4 shows the correction factors in the optimized emissions relative to the prior emissions for anthropogenic fine dust,  $\text{NO}_x$ , and  $\text{SO}_2$  over the North China Plain, and compares the inversion results averaged for November 5–11 (APEC) and October 22–28, 2014. Optimized anthropogenic emissions over the BTH region show on average 21% decreases for fine dust and 4% for  $\text{NO}_x$  in the APEC week. In contrast, emissions in the week of 22–28 October require 9% increases for fine dust and 15% increases for  $\text{NO}_x$ ; both are significantly higher ( $p$ -values  $< 0.05$ ) than those in APEC. Emission reductions for anthropogenic emissions of  $\text{NH}_3$ , BC, and OC follow similar patterns (Figure S6). The emission control measures were effective in Beijing (33%  $\text{NO}_x$  emission reductions), and particularly in Shijiazhuang city of the southern Hebei province (about 80% for fine dust, and 35% for  $\text{NO}_x$ ). For  $\text{SO}_2$ , the optimized emissions show large decreases relative to the prior emissions in the BTH region, but minor emission changes between the two time periods (36% vs 35%) as optimization of the  $\text{SO}_2$  emissions is dominated by the high  $\text{SO}_2$  biases as discussed above.

Our top-down estimates of emission changes (8%–33% reduction among different species in Beijing and 6%–30% over BTH) before and during APEC are similar to yet lower than

the bottom-up estimates by Liu et al.<sup>63</sup> (more than 40% in Beijing and 30% in surround provinces), reflecting the effectiveness of joint regional emission controls for mitigating  $\text{PM}_{2.5}$  pollution over Beijing. The differences can be attributed to uncertainties in both the bottom-up approach such as the actual implementation of emission control measures and the top-down approach such as measurement limits and model errors. In Figure 1, we also show model results from a sensitivity simulation with all anthropogenic emissions over BTH reduced by 30% during APEC. This decrease simulated  $\text{PM}_{2.5}$  concentrations by  $10.6$ – $23.7 \mu\text{g m}^{-3}$  over the BTH cities, roughly correcting the prior model high bias in Beijing during the period.

**3.3. Regional Influence and Transport Time.** We now quantify the sources contributing to the  $\text{PM}_{2.5}$  concentrations in Beijing using the adjoint sensitivity computed with the optimized emissions. Different from source apportionment methods such as backward trajectories<sup>4</sup> and emissions-labeling,<sup>67</sup> the adjoint sensitivity estimates the consequences of emission perturbations around the current model state. Figure 5 shows the sensitivities of daily mean surface  $\text{PM}_{2.5}$  concentrations in Beijing (the grid cell covering the center of Beijing:  $39.9^\circ\text{N}$ ,  $116.3^\circ\text{E}$ ) for three pollution days of October 18, October 25, and November 10 in the year 2014. The left panels show the geographical distribution of the sensitivities integrated over all aerosol primary and precursor emissions at each model grid cell. The right panels show the time-dependent sensitivities (going backward for 120 h) to different aerosol emissions integrated over the model domain, representing the accumulating and transport time of  $\text{PM}_{2.5}$  sources.

As shown in Figure 5, high  $\text{PM}_{2.5}$  on October 18 in Beijing with a simulated daily mean of  $128 \mu\text{g m}^{-3}$  was mainly influenced by dust emissions that account for 71.9% of the total

adjoint sensitivity. These mostly originated from the Gobi Desert in southwestern Mongolia and the Badain Jaran Desert in northern China, and traveled through Inner Mongolia for about 48–72 h before arriving at Beijing. This pattern has been identified as a major transport pathway of dust pollution events in Beijing that are frequently observed in spring and fall.<sup>68,69</sup> There was also a smaller dust plume arriving at Beijing this day originating from the deserts in the western China 4 days ago. Emissions of other species were responsible for the remaining 28.1% of the sensitivity (NH<sub>3</sub>: 5.9%, SO<sub>2</sub>: 3.0%, NO<sub>x</sub>: 4.1%, BC: 2.3%, and OC: 12.8% with 7.8% attributed to SOA), and they were mainly from Beijing local (Beijing municipality) and Hebei province.

The adjoint sensitivities for the two other pollution days: October 25 (248 μg m<sup>-3</sup>) and November 10 (89 μg m<sup>-3</sup>) show significant contributions from secondary inorganic aerosols. The sensitivities to SO<sub>2</sub>, NO<sub>x</sub>, and NH<sub>3</sub> emissions account for nearly half of the total adjoint sensitivities. NH<sub>3</sub> emissions contribute 17.5% and 18.5% of the total sensitivities for the two cases, and NO<sub>x</sub> emissions contribute 15.0% and 14.2%. Contributions from fine dust and OC (including both primary and secondary) sources are also important, with percentage values of 25.8% and 27.6% for fine dust, and 25.0% and 24.6% for OC. The adjoint sensitivities persist backward not only for the pollution day but also in the previous 2 days, reflecting significant accumulation and transport of PM<sub>2.5</sub> to Beijing in the 3-day period. For the October 25 case, Beijing local sources emitted during that day only account for 27% of the total adjoint sensitivity, while sources from Tianjin and Hebei account for 47% and take 6–72 h to arrive at Beijing. Adjoint sensitivities for November 10 have a higher local contribution (39%), and also show strong regional transport influences from the southern Hebei and other sources spreading over the North China Plain.

The high model sensitivity to NH<sub>3</sub> and NO<sub>x</sub> emissions is associated with the nitrate formation in fall and winter. The colder temperature and weaker tropospheric oxidation capability favors formation of aerosol nitrate. Wang et al.<sup>70</sup> found that nitrate concentrations could be more sensitive to NH<sub>3</sub> emissions than NO<sub>x</sub> emissions in wintertime of the North China Plain when nitrate formation was limited by NH<sub>3</sub> emissions. This is the condition here that there are sufficient NO<sub>x</sub> emissions but relatively low NH<sub>3</sub> emissions in fall. High nitrate concentrations were also observed in Beijing during this period,<sup>24,48</sup> e.g., Zhang et al.<sup>24</sup> reported mean aerosol concentrations of 13.6 μg m<sup>-3</sup> for nitrate, 9.8 μg m<sup>-3</sup> for sulfate and 6.8 μg m<sup>-3</sup> for ammonium in Beijing during October 17–November 12, 2015. Our model results well capture the mean concentrations for nitrate (14.5 μg m<sup>-3</sup>), sulfate (9.5 μg m<sup>-3</sup>), and ammonium (7.6 μg m<sup>-3</sup>). Although NO<sub>x</sub> and its oxidation product HNO<sub>3</sub> have relatively short lifetimes and do not transport a long distance, by reacting with NH<sub>3</sub> and forming aerosol ammonium nitrate that has a longer lifetime, their regional influences are increased.

While this study used model simulations with assimilated surface measurements of PM<sub>2.5</sub> and SO<sub>2</sub>, such data is still limited with regards to aerosol composition to quantify contributions from different primary and precursor sources. Future developments will target assimilation of more measurements into the model to provide additional constraints on the sources of primary and secondary aerosols, such as measurements of aerosol composition, satellite observations of NO<sub>2</sub>, and aerosol optical depths (AOD). We have also shown here

that assimilation of atmospheric composition measurements using the adjoint model can largely improve the model simulation, which can be valuable for near-real-time data analyses and air quality forecasts.

## ■ ASSOCIATED CONTENT

### 📄 Supporting Information

The Supporting Information is available free of charge on the ACS Publications website at DOI: 10.1021/acs.est.6b03010.

Figures S1. Domain of the study over North China; Figure S2. Anthropogenic emissions of SO<sub>2</sub>, NO<sub>x</sub>, NH<sub>3</sub>, black carbon (BC), organic carbon (OC), and fine dust over North China; Figure S3. OMI observed and GEOS-Chem simulated NO<sub>2</sub> tropospheric columns over North China; Figure S4. Surface mass concentrations of SO<sub>2</sub> averaged over two weeks; Figure S5. Evolution of surface PM<sub>2.5</sub> concentrations over the North China Plain; and Figure S6. Correction factors in the optimized anthropogenic emissions of BC, OC, and NH<sub>3</sub> relative to the prior emissions (PDF)

## ■ AUTHOR INFORMATION

### Corresponding Author

\*Phone: +86-10-6276-6709; fax: +86-10-6275-1094; e-mail: zhanglg@pku.edu.cn (L.Z.).

### Notes

The authors declare no competing financial interest.

## ■ ACKNOWLEDGMENTS

This work was supported by China's National Basic Research Program (2014CB441303), and by the National Natural Science Foundation of China (41205103 and 41475112). D.K.H. recognizes support from NASA NNX13AK86G.

## ■ REFERENCES

- (1) Chan, C. K.; Yao, X. Air pollution in mega cities in China. *Atmos. Environ.* **2008**, *42*, 1–42.
- (2) Zhang, R.; Wang, G.; Guo, S.; Zamora, M. L.; Ying, Q.; Lin, Y.; Wang, W.; Hu, M.; Wang, Y. Formation of Urban Fine Particulate Matter. *Chem. Rev.* **2015**, *115*, 3803–3855.
- (3) Huang, R.; Zhang, Y.; Bozzetti, C.; Ho, K.; Cao, J.; et al. High secondary aerosol contribution to particulate pollution during haze events in China. *Nature* **2014**, *514*, 218–222.
- (4) Zhang, R.; Jing, J.; Tao, J.; Hsu, S. C.; Wang, G.; Cao, J.; Lee, C. S. L.; Zhu, L.; Chen, Z.; Zhao, Y.; Shen, Z. Chemical characterization and source apportionment of PM<sub>2.5</sub> in Beijing: seasonal perspective. *Atmos. Chem. Phys.* **2013**, *13*, 7053–7074.
- (5) Wang, L. T.; Wei, Z.; Yang, J.; Zhang, Y.; Zhang, F. F.; Su, J.; Meng, C. C.; Zhang, Q. The 2013 severe haze over southern Hebei, China: model evaluation, source apportionment, and policy implications. *Atmos. Chem. Phys.* **2014**, *14*, 3151–3173.
- (6) Wang, Y.; Zhang, Q.; Jiang, J.; Zhou, W.; Wang, B.; He, K.; Duan, F.; Zhang, Q.; Philip, S.; Xie, Y. Enhanced sulfate formation during China's severe winter haze episode in January 2013 missing from current models. *J. Geophys. Res.* **2014**, *119*, 10425–10440.
- (7) Pope, I. C. A.; Dockery, D. W. Health effects of fine particulate air pollution: lines that connect. *J. Air Waste Manage. Assoc.* **2006**, *56*, 709–742.
- (8) Krewski, D.; Jerrett, M.; Burnett, R. T.; Ma, R.; Hughes, E.; Shi, Y.; Turner, M. C.; Pope, C. A., III; Thurston, G.; Calle, E. E.; Thun, M. J. Extended Follow-Up and Spatial Analysis of the American Cancer Society Study Linking Particulate Air Pollution and Mortality. *HEI Research Report 140*; Health Effects Institute: Boston, MA, 2009.

- (9) Lelieveld, J.; Evans, J. S.; Fnais, M.; Giannadaki, D.; Pozzer, A. The contribution of outdoor air pollution sources to premature mortality on a global scale. *Nature* **2015**, *525*, 367–371.
- (10) Zhang, X. Y.; Wang, Y. Q.; Niu, T.; Zhang, X. C.; Gong, S. L.; Zhang, Y. M.; Sun, J. Y. Atmospheric aerosol compositions in China: spatial/temporal variability, chemical signature, regional haze distribution and comparisons with global aerosols. *Atmos. Chem. Phys.* **2012**, *12*, 779–799.
- (11) Rosenfeld, D.; Sherwood, S.; Wood, R.; Donner, L. Climate Effects of Aerosol-Cloud Interactions. *Science* **2014**, *343*, 379–380.
- (12) Zhang, H.; Wang, S.; Hao, J.; Wang, X.; Wang, S.; Chai, F.; Li, M. Air pollution and control action in Beijing. *J. Cleaner Prod.* **2016**, *112*, 1519–1527.
- (13) Chinese State Council, Action Plan on Air Pollution Prevention and Control, 2013 (in Chinese) ([http://www.gov.cn/zwggk/2013-09/12/content\\_2486773.htm](http://www.gov.cn/zwggk/2013-09/12/content_2486773.htm), accessed on 1 November 2015).
- (14) Li, P.; Yan, R.; Yu, S.; Wang, S.; Liu, W.; Bao, H. Reinstatement regional transport of PM<sub>2.5</sub> as a major cause of severe haze in Beijing. *Proc. Natl. Acad. Sci. U. S. A.* **2015**, *112*, E2739–E2740.
- (15) Zhang, L.; Liu, L.; Zhao, Y.; Gong, S.; Zhang, X.; Henze, D. K.; Capps, S. L.; Fu, T. M.; Zhang, Q.; Wang, Y. Source attribution of particulate matter pollution over North China with the adjoint method. *Environ. Res. Lett.* **2015**, *10*, 084011.
- (16) Guo, S.; Hu, M.; Zamora, M. L.; Peng, J.; Shang, D.; Zheng, J.; Du, Z.; Wu, Z.; Shao, M.; Zeng, L.; Molina, M. J.; Zhang, R. Elucidating severe urban haze formation in China. *Proc. Natl. Acad. Sci. U. S. A.* **2014**, *111*, 17373–17378.
- (17) Wang, Y.; McElroy, M. B.; Boersma, K. F.; Eskes, H. J.; Veefkind, J. P. Traffic restrictions associated with the Sino-African summit: Reductions of NO<sub>x</sub> detected from space. *Geophys. Res. Lett.* **2007**, *34*, L08814.
- (18) Cheng, Y. F.; Heintzenberg, J.; Wehner, B.; Wu, Z. J.; Su, H.; Hu, M.; Mao, J. T. Traffic restrictions in Beijing during the Sino-African Summit 2006: aerosol size distribution and visibility compared to long-term in situ observations. *Atmos. Chem. Phys.* **2008**, *8*, 7583–7594.
- (19) Streets, D. G.; Fu, J. S.; Jang, C. J.; Hao, J.; He, K.; Tang, X.; Zhang, Y.; Wang, Z.; Li, Z.; Zhang, Q.; Wang, L.; Wang, B.; Yu, C. Air quality during the 2008 Beijing Olympic Games. *Atmos. Environ.* **2007**, *41*, 480–492.
- (20) Wang, Y.; Hao, J.; McElroy, M. B.; Munger, J. W.; Ma, H.; Chen, D.; Nielsen, C. P. Ozone air quality during the 2008 Beijing Olympics: effectiveness of emission restrictions. *Atmos. Chem. Phys.* **2009**, *9*, 5237–5251.
- (21) Wang, S.; Zhao, M.; Xing, J.; Wu, Y.; Zhou, Y.; Lei, Y.; He, K.; Fu, L.; Hao, J. Quantifying the Air Pollutants Emission Reduction during the 2008 Olympic Games in Beijing. *Environ. Sci. Technol.* **2010**, *44* (7), 2490–2496.
- (22) Wang, T.; Nie, W.; Gao, J.; et al. Air quality during the 2008 Beijing Olympics: secondary pollutants and regional impact. *Atmos. Chem. Phys.* **2010**, *10*, 7603–7615.
- (23) Li, J.; Xie, S. D.; Zeng, L. M.; Li, L. Y.; Li, Y. Q.; Wu, R. R. Characterization of ambient volatile organic compounds and their sources in Beijing, before, during, and after Asia-Pacific Economic Cooperation China 2014. *Atmos. Chem. Phys.* **2015**, *15*, 7945–7959.
- (24) Zhang, J. K.; Wang, L. L.; Wang, Y. H.; Wang, Y. S. Submicron aerosols during the Beijing Asia-Pacific Economic Cooperation conference in 2014. *Atmos. Environ.* **2016**, *124*, 224–231.
- (25) Henze, D. K.; Hakami, A.; Seinfeld, J. H. Development of the adjoint of GEOS-Chem. *Atmos. Chem. Phys.* **2007**, *7*, 2413–2433.
- (26) Chen, D.; Wang, Y. X.; McElroy, M. B.; He, K.; Yantosca, R. M.; Le Sager, P. Regional CO pollution in China simulated by high-resolution nested-grid GEOS-Chem model. *Atmos. Chem. Phys.* **2009**, *9*, 3825–3839.
- (27) Kim, P. S.; Jacob, D. J.; Fisher, J. A.; et al. Sources, seasonality, and trends of southeast US aerosol: an integrated analysis of surface, aircraft, and satellite observations with the GEOS-Chem chemical transport model. *Atmos. Chem. Phys.* **2015**, *15*, 10411–10433.
- (28) Park, R. J.; Jacob, D. J.; Field, B. D.; Yantosca, R. M.; Chin, M. Natural and transboundary pollution influences on sulfate-nitrate-ammonium aerosols in the United States: Implications for policy. *J. Geophys. Res.* **2004**, *109*, D15204.
- (29) Mao, J.; Fan, S.; Jacob, D. J.; Travis, K. R. Radical loss in the atmosphere from Cu-Fe redox coupling in aerosols. *Atmos. Chem. Phys.* **2013**, *13*, 509–519.
- (30) Jacob, D. J. Heterogeneous chemistry and tropospheric ozone. *Atmos. Environ.* **2000**, *34*, 2131–2159.
- (31) Martin, R. V.; Jacob, D. J.; Yantosca, R. M.; Chin, M.; Ginoux, P. Global and regional decreases in tropospheric oxidants from photochemical effects of aerosols. *J. Geophys. Res.* **2003**, *108* (D3), 4097.
- (32) Binkowski, F. S.; Roselle, S. J. Models 3 Community Multiscale Air Quality (CMAQ) model aerosol component 1. Model description. *J. Geophys. Res.* **2003**, *108* (D6), 4183.
- (33) Chin, M.; Ginoux, P.; Kinne, S.; Torres, O.; Holben, B. N.; Duncan, B. N.; Martin, R. V.; Logan, J. A.; Higurashi, A. Tropospheric aerosol optical thickness from the GOCART model and comparisons with satellite and Sun photometer measurements. *J. Atmos. Sci.* **2002**, *59* (3), 461–483.
- (34) Park, R.; Jacob, D.; Kumar, N.; Yantosca, R. Regional visibility statistics in the United States: Natural and transboundary pollution influences, and implications for the Regional Haze Rule. *Atmos. Environ.* **2006**, *40*, 5405–5423.
- (35) Fairlie, D. T.; Jacob, D. J.; Park, R. J. The impact of transpacific transport of mineral dust in the United States. *Atmos. Environ.* **2007**, *41*, 1251–1266.
- (36) Liu, H.; Jacob, D. J.; Isabelle, B.; Yantosca, R. M. Constraints from <sup>210</sup>Pb and <sup>7</sup>Be on wet deposition and transport in a global three-dimensional chemical tracer model driven by assimilated meteorological fields. *J. Geophys. Res.* **2001**, *106* (D11), 12109–12128.
- (37) Wesely, M. Parameterization of surface resistances to gaseous dry deposition in regional-scale numerical models. *Atmos. Environ.* **1989**, *23*, 1293–1304.
- (38) Zhang, L. M.; Gong, S. L.; Padro, J.; Barrie, L. A size-segregated particle dry deposition scheme for an atmospheric aerosol module. *Atmos. Environ.* **2001**, *35* (3), 549–560.
- (39) Zhang, L.; Jacob, D. J.; Knipping, E. M.; Kumar, N.; Munger, J. W.; Carouge, C. C.; van Donkelaar, A.; Wang, Y. X.; Chen, D. Nitrogen deposition to the United States: distribution, sources, and processes. *Atmos. Chem. Phys.* **2012**, *12*, 4539–4554.
- (40) Zhang, L.; Jacob, D. J.; Yue, X.; Downey, N. V.; Wood, D. A.; Blewitt, D. Sources contributing to background surface ozone in the US Intermountain West. *Atmos. Chem. Phys.* **2014**, *14*, 5295–5309.
- (41) Zhang, Q.; Streets, D. G.; Carmichael, G. R.; He, K. B.; Huo, H.; Kannari, A.; Klimont, Z.; Park, I. S.; Reddy, S.; Fu, J. S. Asian emissions in 2006 for the NASA INTEX-B mission. *Atmos. Chem. Phys.* **2009**, *9* (14), 5131–5153.
- (42) Lei, Y.; Zhang, Q.; He, K. B.; Streets, D. G. Primary anthropogenic aerosol emission trends for China, 1990–2005. *Atmos. Chem. Phys.* **2011**, *11*, 931–954.
- (43) Kurokawa, J.; Ohara, T.; Morikawa, T.; Hanayama, S.; Janssens-Maenhout, G.; Fukui, T.; Kawashima, K.; Akimoto, H. Emissions of air pollutants and greenhouse gases over Asian regions during 2000–2008: Regional Emission inventory in Asia (REAS) version 2. *Atmos. Chem. Phys.* **2013**, *13*, 11019–11058.
- (44) Zhao, Y.; Zhang, L.; Pan, Y.; Wang, Y.; Paulot, F.; Henze, D. K. Atmospheric nitrogen deposition to the northwestern Pacific: seasonal variation and source attribution. *Atmos. Chem. Phys.* **2015**, *15*, 10905–10924.
- (45) Zhu, L.; Henze, D. K.; Cady-Pereira, K. E.; Shephard, M. W.; Luo, M.; Pinder, R. W.; Bash, J. O.; Jeong, G.-R. Constraining U.S. ammonia emissions using TES remote sensing observations and the GEOS-Chem adjoint model. *J. Geophys. Res.* **2013**, *118*, 3355–3368.
- (46) Fu, T.-M.; Cao, J. J.; Zhang, X. Y.; et al. Carbonaceous aerosols in China: top-down constraints on primary sources and estimation of secondary contribution. *Atmos. Chem. Phys.* **2012**, *12*, 2725–2746.

- (47) Pye, H. O. T.; Chan, A. W. H.; Barkley, M. P.; Seinfeld, J. H. Global modeling of organic aerosol: the importance of reactive nitrogen ( $\text{NO}_x$  and  $\text{NO}_3$ ). *Atmos. Chem. Phys.* **2010**, *10*, 11261–11276.
- (48) Sun, Y.; Wang, Z.; Wild, O.; et al. "APEC Blue": Secondary Aerosol Reductions from Emission Controls in Beijing. *Sci. Rep.* **2016**, *6*, 20668.
- (49) Riva, M.; Tomaz, S.; Cui, T.; Lin, Y. H.; Perraudin, E.; Gold, A.; Stone, E. A.; Villenave, E.; Surratt, J. D. Evidence for an unrecognized secondary anthropogenic source of organosulfates and sulfonates: gas-phase oxidation of polycyclic aromatic hydrocarbons in the presence of sulfate aerosol. *Environ. Sci. Technol.* **2015**, *49*, 6654–6664.
- (50) Lee, B. H.; Mohr, C.; et al. Highly functionalized organic nitrates in the southeast united states: contribution to secondary organic aerosol and reactive nitrogen budgets. *Proc. Natl. Acad. Sci. U. S. A.* **2016**, *113* (6), 1516–1521.
- (51) Heald, C. L.; Collett, J. L., Jr; Lee, T.; et al. Atmospheric ammonia and particulate inorganic nitrogen over the United States. *Atmos. Chem. Phys.* **2012**, *12* (21), 10295–10312.
- (52) Wang, Y.; Zhang, Q. Q.; He, K.; Zhang, Q.; Chai, L. Sulfate-nitrate-ammonium aerosols over China: response to 2000–2015 emission changes of sulfur dioxide, nitrogen oxides, and ammonia. *Atmos. Chem. Phys.* **2013**, *13*, 2635–2652.
- (53) Henze, D. K.; Seinfeld, J. H.; Shindell, D. T. Inverse modeling and mapping US air quality influences of inorganic PM<sub>2.5</sub> precursor emissions using the adjoint of GEOS-Chem. *Atmos. Chem. Phys.* **2009**, *9*, 5877–5903.
- (54) Kharol, S. K.; Martin, R. V.; Philip, S.; Vogel, S.; Henze, D. K.; Chen, D.; Wang, Y.; Zhang, Q.; Heald, C. L. Persistent sensitivity of Asian aerosol to emissions of nitrogen oxides. *Geophys. Res. Lett.* **2013**, *40*, 1021–1026.
- (55) Wang, J.; Xu, X.; Henze, D. K.; Zeng, J.; Ji, Q.; Tsay, S. C.; Huang, J. Top-down estimate of dust emissions through integration of MODIS and MISR aerosol retrievals with the GEOS-Chem adjoint model. *Geophys. Res. Lett.* **2012**, *39* (8), L08802.
- (56) Lamsal, L. N.; Martin, R. V.; van Donkelaar, A.; Steinbacher, M.; Celarier, E. A.; Bucsel, E.; Dunlea, E. J.; Pinto, J. P. Ground-level nitrogen dioxide concentrations inferred from the satellite-borne Ozone Monitoring Instrument. *J. Geophys. Res.* **2008**, *113*, D16308.
- (57) Heald, C. L.; Jacob, D. J.; Jones, D. B. A.; Palmer, P. I.; Logan, J. A.; Streets, D. G.; Sachse, G. W.; Gille, J. C.; Hoffman, R. N.; Nehr Korn, T. Comparative inverse analysis of satellite (MOPITT) and aircraft (TRACE-P) observations to estimate Asian sources of carbon monoxide. *J. Geophys. Res.* **2004**, *109*, D23306.
- (58) Byrd, R. H.; Lu, P. H.; Nocedal, J.; Zhu, C. Y. A limited memory algorithm for bound constrained optimization. *SIAM J. Sci. Comput.* **1995**, *16* (5), 1190–1208.
- (59) Lu, Z.; Zhang, Q.; Streets, D. G. Sulfur dioxide and primary carbonaceous aerosol emissions in China and India, 1996–2010. *Atmos. Chem. Phys.* **2011**, *11*, 9839–9864.
- (60) Zhao, Y.; Zhang, J.; Nielsen, C. P. The effects of recent control policies on trends in emissions of anthropogenic atmospheric pollutants and  $\text{CO}_2$  in China. *Atmos. Chem. Phys.* **2013**, *13*, 487–508.
- (61) Wang, T.; Hendrick, F.; Wang, P.; et al. Evaluation of tropospheric  $\text{SO}_2$  retrieved from MAX-DOAS measurements in Xianghe, China. *Atmos. Chem. Phys.* **2014**, *14*, 11149–11164.
- (62) Zheng, B.; Zhang, Q.; Zhang, Y.; He, K. B.; Wang, K.; Zheng, G. J.; Duan, F. K.; Ma, Y. L.; Kimoto, T. Heterogeneous chemistry: a mechanism missing in current models to explain secondary inorganic aerosol formation during the January 2013 haze episode in North China. *Atmos. Chem. Phys.* **2015**, *15*, 2031–2049.
- (63) Liu, J. G.; Xie, P.; Wang, Y. S.; Wang, Z. F.; He, H.; Liu, W. Haze Observation and Control Measure Evaluation in Jing-Jin-Ji (Beijing, Tianjin, Hebei) Area during the Period of the Asia-Pacific Economic Cooperation (APEC) Meeting. *Bulletin of the Chinese Academy of Sciences* **2015**, *30* (3), 368–377.
- (64) Huang, K.; Zhang, X.; Lin, Y. The "APEC Blue" phenomenon: Regional emission control effects observed from space. *Atmos. Res.* **2015**, *164–165*, 65–75.
- (65) Zhang, Y.; Sperber, K. R.; Boyle, J. S. Climatology and Interannual Variation of the East Asian Winter Monsoon: Results from the 1979–95 NCEP/NCAR Reanalysis. *Mon. Weather Rev.* **1997**, *125*, 2605–2619.
- (66) Liu, H.; Jacob, D. J.; Isabelle, B.; Yantosca, R. M.; Duncan, B. N.; Sachse, G. W. Transport pathways for Asian pollution outflow over the Pacific: Interannual and seasonal variations. *J. Geophys. Res.* **2003**, *108* (D20), 8786.
- (67) Zhang, H.; Li, J.; Ying, Q.; Yu, J. Z.; Wu, D.; Cheng, Y.; He, K.; Jiang, J. Source apportionment of PM<sub>2.5</sub> nitrate and sulfate in China using a source-oriented chemical transport model. *Atmos. Environ.* **2012**, *62*, 228–242.
- (68) Zhang, X. Y.; Gong, S. L.; Shen, Z. X.; Mei, F. M.; Xi, X. X.; Liu, L. C.; Zhou, Z. J.; Wang, D.; Wang, Y. Q.; Cheng, Y. Characterization of soil dust aerosol in China and its transport and distribution during 2001 ACE-Asia: 1. Network observations. *J. Geophys. Res.* **2003**, *108* (D9), 4261.
- (69) Wang, Y. Q.; Zhang, X. Y.; Arimoto, R.; Cao, J. J.; Shen, Z. X. The transport pathways and sources of PM<sub>10</sub> pollution in Beijing during spring 2001, 2002 and 2003. *Geophys. Res. Lett.* **2004**, *31*, L14110.
- (70) Wang, S.; Xing, J.; Jang, C.; Zhu, Y.; Fu, J. S.; Hao, J. Impact assessment of ammonia emissions on inorganic aerosols in East China using response surface modeling technique. *Environ. Sci. Technol.* **2011**, *45* (21), 9293–9300.